Poly(2-Oxazoline)-Based Magnetic Hydrogels: Synthesis, Performance and Cytotoxicity

Martin Cvek,[1*] Anna Zahoranova,[2*] Miroslav Mrlik,[1] Petra Sramkova,[2] Antonin Minarik,[1,3]

Michal Sedlacik[1]

[1]*Centre of Polymer Systems, University Institute, Tomas Bata University in Zlín, Trida T. Bati 5678, 760 01 Zlín, Czech Republic*

[2]*Polymer Institute, Slovak Academy of Sciences, Dubravska cesta 9, 845 41 Bratislava, Slovakia*

[3]*Department of Physics and Materials Engineering, Faculty of Technology, Tomas Bata University in Zlín, Vavreckova 275, 760 01 Zlín, Czech Republic*

*Authors to whom correspondence should be addressed:

cvek@utb.cz

anna.zahoranova@savba.sk

Abstract. The research of smart biomaterials is one of the cornerstones in tissue engineering and regenerative medicine. Here, we report on the development of magnetic hydrogels combining high biocompatibility and remarkable activity in magnetic fields. The poly(2-ethyl-2-oxazoline) (POx)-based magnetic hydrogels were fabricated via living ring-opening cationic polymerization with *in-situ* embedding the carbonyl iron (CI) particles. The effects of the CI concentration on magnetic, viscoelastic/magnetorheological properties, equilibrium swelling degree, and cytotoxicity were investigated. The hydrogels exhibited open pore structure as proved by computed tomography (CT) imaging. The susceptibility measurements revealed the concentration-dependent field-induced particle re-structuration identifying the elongation/contraction of the material, which determines a potential for the magneto-mechanical stimulation of cells. The POx-based magnetic hydrogels possessed the amphiphilic character, and decreasing liquid-holding capability with increasing CI concentration. The

1

viscoelastic measurements suggested the particle/matrix interaction, most likely through a coordination complex formation, based on the inconsistency of the experimental storage modulus with the Krieger–Dougherty theory. The synthesized materials exhibited excellent biocompatibility towards 3T3 fibroblast cell line in both, the extract toxicity and direct contact cytotoxicity tests (ISO standards). The unique combination of properties, represented by magneto-mechanical activity and biocompatibility, could be favorable in biomedicine, biomechanics and related fields.

Keywords: magnetic gel; living cationic polymerization; composite; poly(2-oxazoline); cytotoxicity; magnetorheology; biomedical application

Graphical abstract
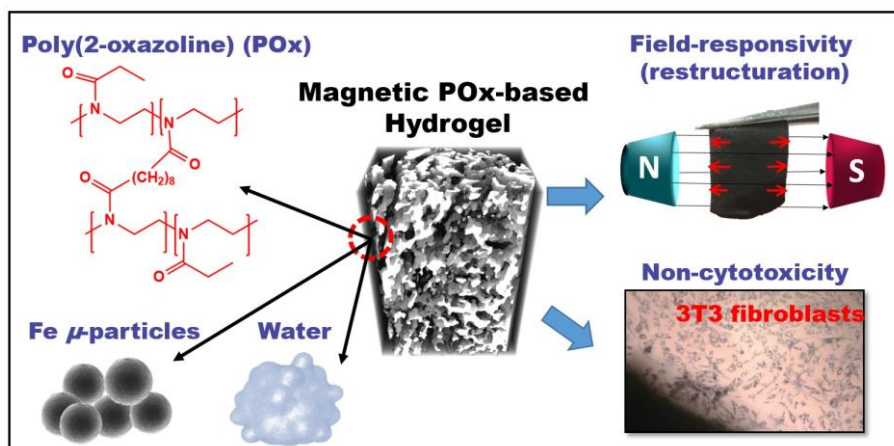
1. Introduction

Hydrogels are three-dimensional cross-linked polymer networks carrying large amounts of water in their structure. They have been, over the past decades, extensively applied in biomedical fields due to their functional properties such as water-binding capacity, high swelling degree, good biocompatibility, or synergistic features with other materials [1-3]. For instance, hybridization of hydrogels with specific mineral-based inorganic substances provides materials suitable for biomimetic mineralization [3]. Combining the hydrogels with magnetic nanoparticles or micro-particles creates the additional capabilities including magnetic field-controlled mechanical properties [1,2]. Besides that, magnetic gels are popular in thermal therapy triggered by the alternating magnetic fields to eradicate cancer cells. When loaded with specific drugs, they can be used for controlled drug release [1,4]. Magnetic hydrogels can also mimic some functions of soft body tissues such as contraction/elongation, electrocapacity etc.[5,6]

Design of biomaterials including the hydrogels is generally a complex issue. For a successful fabrication of magnetic gels that resemble the human body tissue, the selection of the materials is a challenging task. To this day, various polymers have been used as a matrix of magnetic hydrogels, e.g. carrageenan [7], chitosan [4], polyvinyl alcohol [8], polyurethanes [9], polyacrylamide [1,5,10], agarose [2] or alginate [11]. Apart from these 'conventional' polymers, poly(2-oxazoline)s (POx) have been recognized as an upcoming platform to design different kinds of polymer-based biomaterials [12].

Poly(2-oxazoline)s are pseudo-polypeptides accessible via living cationic ring-opening polymerization of 2-oxazolines. In the context of *in vivo* applications, tertiary amide groups in the POx are not readily recognized and hydrolyzed by enzymes, thus they show an improved stability in biological environments [13]. Moreover, regardless the different alkyl chain lengths, the POx exhibit low cytotoxicity and do not stimulate, neither affect the functionality of the

immune cells when tested *in vitro* [14]. In our preceding paper [15], a broad series of the POx-based hydrogels was prepared using different chain-length cross-linking agents, such as 1,4-butylene-2,2'-bis(2-oxazoline), 1,6-hexamethylene-2,2'-bis(2-oxazoline) or 1,8-octamethylene-2,2'-bis(2-oxazoline), and various monomer-to-cross-linker molar ratios. As will be discussed further, the obtained database of results allowed selecting the suitable matrix in terms of mechanical properties and cell viability, for subsequent embedding of magnetic particles.

In the research of magnetic hydrogels, different types of particles have been used as magnetically-active component. Recent candidates are represented by magnetite (Fe_3O_4) in a neat form [4,7,8] or acting as the core with SiO_2 capping layer [1], close-to-maghemite particles ($Fe_{2.04}O_{2.96}$) with bimodal size distribution [5], or barium ferrites ($BaFe_{12}O_{19}$) either as nanoparticles [10] or their micron-sized analogues [7]. The biological fate, clearance time, and particle biodistribution after the incorporation into a living organism are strongly affected by the particle size [16]. Moreover, the particle size determines their response to magnetic forces, although the particle size is not the single relevant factor. Generally, the interactions among small (below 50 nm) particles are dominated by thermal motion, which limits the performance of their gels in magnetic fields. On the contrary, larger particles (micron-sized) such as the carbonyl iron (CI) particles, provide stronger magnetic response, but they are prone to sedimentation during the hydrogel preparation leading to possible heterogeneities in the material [2]. These drawbacks can be avoided by optimizing the fabrication process, and the preparation of magnetic hydrogels with the embedded CI micro-particles can be performed [9,17,18]. However, in none of these articles, the effect of the CI particles on the cytotoxicity of their hydrogels was presented.

In this study, we report on the synthesis, physical and biological testing of novel POx-based magnetic hydrogels with embedded CI particles. The POx-based matrix was designed

considering the data by Zahoranova et al.[15] using the 1,8-octamethylene-2,2´-bis(2-oxazoline) as a cross-linking agent. The goal of this work was to determinate the physicochemical properties of the POx-based hydrogels upon the introduction of various amounts of the CI particles. The structure of the synthesized materials was evaluated using scanning electron microscopy and computer tomography, followed by swelling and magnetic and magnetorheological (MR) investigations. Finally, we analyzed the *in vitro* cytotoxicity of the POx-based magnetic hydrogels according to the ISO standards.

2. Experimental section

2.1 Synthesis of 1,8-octamethylene-2,2´-bis(2-oxazoline) cross-linker. The synthesis of 1,8-octamethylene-2,2´-bis(2-oxazoline) (OctBisOx) cross-linking agent was inspired by a procedure reported by Nery et al.[19]. Briefly, sebacoyl chloride (4.46 mL, 20.9 mmol) dissolved in tetrachloromethane (60 mL) was drop-wise added into the mixture of potassium hydroxide (KOH, 7.1 g, 125.5 mmol) and 2-chloroethylamine hydrochloride (6.1 g, 52.3 mmol) in distilled water (50 mL) at the temperature of 0°C. The mixture was stirred overnight at laboratory temperature. The white precipitate was filtered off and dried under reduced pressure at 40°C (yield of 6.81 g, near to 100%). To perform the cyclization, *N,N'*-bis(2-chloroethyl)sebacamide (14 g, 43.2 mmol) was dissolved together with KOH (6.1 g, 108.1 mmol) in methanol (200 mL) and refluxed for 6 h. The salt (potassium chloride) was filtered off, and methanol was gently evaporated. The product was dissolved in chloroform, and washed with saturated aqueous NaCl solution (2×50 mL). Subsequently, chloroform was evaporated, and the product was dried at 40°C for two days under reduced pressure. The product was obtained as white powder (yield of 7.56 g, 69%). The chemical structure of the cross-linker was confirmed via ^{1}H NMR analysis using Varian VXR-400 spectrometer (Varian, USA) in DMSO-d6 solutions using tetramethylsilane (TMS) as an internal standard at laboratory

temperature. The ^{1}H NMR spectrum showing the structure and the purity of the product is attached as Supporting Information (Fig. S1).

^{1}H NMR (400 MHz, DMSO-d6, δ): 4.08 (t, 4H; CH$_2$–O), 3.64 (t, 4H; CH$_2$–N), 2.14 (t, 4H; CH$_2$), 1.48 (m, 4H; CH$_2$), 1.22 (m, 8H; CH$_2$–CH$_2$).

2.2 Synthesis of POx-based hydrogels and their magnetic analogues. The neat POx-based hydrogels and their magnetic analogues were prepared via copolymerization of 2-ethyl-2-oxazoline (EtOx) with synthesized OctBisOx (Fig. 1). All the gels were based on the EtOx:OctBisOx molar ratio of 98:2. As will be described further, this ratio was carefully chosen considering the final properties of the product.

To prepare neat POx-based gels, OctBisOx (75.7 mg, 0.3 mmol), methyl 4-nitrobenzenesulfonate (MeONs, 32.6 mg, 0.15 mmol) were placed into a Schlenk flask and dried under vacuum for 45 min. Subsequently, EtOx (1.46 g, 14.7 mmol) and benzonitrile (2 mL) were added and the mixture was stirred for 4 h at 110°C in an oil bath. The reaction was performed under inert atmosphere (N$_2$) using a glove box (LABstar glove box, MBraun, Germany).

In the case of magnetic hydrogels, different amounts of the CI micro-particles (0.8, 1.6, and 2.4 g) were added into the reaction mixture together with MeONs and OctBisOx. After the addition of liquid compounds, the mixture was thoroughly stirred for 30 min at 110°C using mechanical stirrer. As this point, the viscosity of the reaction mixture was high enough to prevent the particle sedimentation, but below the gelation point (the stirrer was removed without causing a mechanical damage to the product). After the addition of the CI particles, the system was thoroughly mixed, and the reaction proceeded for additional 3.5 h to finalize the gelation process. As the last step, the products were immersed into an excess of methanol (48 h) and

ethanol (48 h), while each purification agent was changed daily. The latter agent was also used as a storing medium to prevent corrosion of the CI particles.
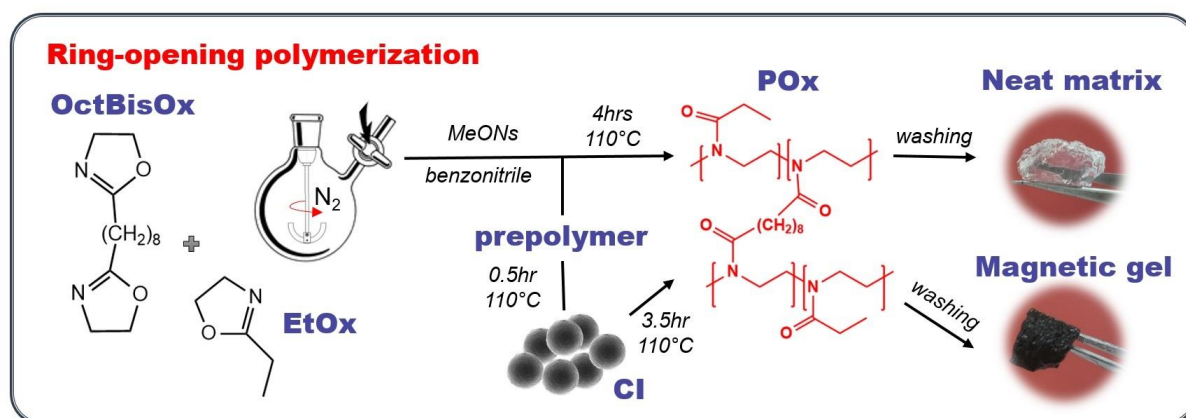

Fig. 1: Reaction scheme for the synthesis of POx gels and their magnetic analogues via living cationic ring-opening polymerization.

The determination of polymerization kinetics was performed in a similar manner. The MeONs (32.6 mg, 0.15 mmol), either with dispersed CI particles (1.6 g) or without the particles, was pre-dried in the Schlenk flask, and transferred to the glove box. Subsequently, benzonitrile (2 mL) and EtOx (1.46 g, 14.7 mmol) were added into the reaction mixture. The assembly was heated to 110°C, and the reaction conversion, C, was analyzed in the pre-selected time intervals. During the polymerization, the both systems were thoroughly mixed using the mechanical stirrer. The C value was estimated via ^{1}H NMR analysis performed on Varian VXR-400 spectrometer (Varian, USA) in CDCl$_3$ solutions using TMS as an internal standard at laboratory temperature.

2.3 Study of swelling. The swelling behavior was characterized via gravimetric analysis in four different solvents, i.e., distilled water, ethanol, dichloromethane, and phosphate buffered saline (PBS). Prior to the analysis, weight of the POx-based freeze-dried gels and their magnetic analogues was monitored. Subsequently, the samples were immersed into an excess on the

corresponding liquid at laboratory temperature, and equilibrated for 24 h. After this time period, no additional swelling was observed. Finally, the samples were gently dried using a paper tissue to remove remaining traces of liquid from their surface and weighted. The equilibrium swelling degree (SD) was calculated according to the following equation (Eq. 1):

$$SD = \frac{w_{sw} - w_d}{w_d} \qquad (1)$$

where w_{sw} is the weight of the swollen sample, and w_d is the weight of its freeze-dried analogue. The SD values were expressed as mean value and standard deviation from the triplicates.

2.4 Scanning electron microscopy. As some analyzes could not be performed in the hydrated state, the POx-based hydrogels were equilibrated in water and freeze-dried. The elimination of water content was performed using CoolSafe 110-4 Pro (LaboGene, Denmark) at the temperature of -110°C, and a pressure of 0.140 hPa, overnight. Subsequently, the samples were metalized with a thin layer of gold using the Bio-Rad sputter coater (E 5000S, Polaron/Quorum, UK). Their internal structure was studied via scanning electron microscopy (SEM) with the help of TS 5136 MM microscope (Tescan, Czech Republic) operating at the accelerating voltage of 20 kV. The device was equipped with a secondary electron detector for SEM, and the INCA x-act detector (51-ADD0007, Oxford Instruments, UK) for the energy dispersive X-ray spectroscopy (EDX).

2.5 Computed tomography. The porosity of the representative water-equilibrated POx-based hydrogel, and its freeze-died analogue was analyzed using an X-ray computed micro-tomography (CT) with the help of SkyScan (Model 1174, Bruker, USA). The device was equipped with the X-ray source, (voltage of 20–50 kV, maximum power of 40W), and the X-ray detector. The CCD 1.3 Mpix was coupled to scintillator by lens with 1:6 zoom range. The projection images were recorded at angular increments of 0.3° using tube voltage, and tube

current of 35–40 kV, and 585–730 μA, respectively. The exposure time was set to 15–30s without using any filter. The 3D reconstructions were performed via built-in CT image analysis software (version 1.16.4.1, Bruker, USA). The results, in terms of total porosity, are expressed as the average and standard deviation from three different cylindrical sections. The representative cross-sectional images of 2.27 mm in diameter, and 3 mm in height were exported from DataViewer software. The distribution of the pore areas was analyzed using ImageJ software (version 1.8, National Institutes of Health, USA) at five different horizontal sections.

2.6 Vibrating-sample magnetometry. The magnetic properties of the hydrogels with embedded CI particles were studied using a vibrating-sample magnetometry (VSM) (Model 7404, Lake Shore, USA) in the magnetic fields approaching to ±15 kOe at laboratory conditions. The samples in the form of thin films were equilibrated in water, wrapped and carefully accommodated into the VSM sample holder (730931 Kel-F, powder/bulk upper/bottom cup), thus their evaporation was prevented.

2.7 Viscoelasticity and magnetorheology. The viscoelastic measurements were carried out on a Physica rheometer (MCR502, Anton Paar, Austria) equipped with the magneto-cell (MRD 180/1T), and a titanium parallel-plate geometry (PP20/MRD/Ti) having 20 mm in a diameter. First, the strain sweeps were recorded at a constant frequency of 1 Hz, while the strain amplitude was varied from 10^{-2} to 2×10^{1} % to determine the existence of the linear viscoelastic region (LVR). Afterwards, the frequency sweeps were performed in a range from 6×10^{-1} to 6×10^{1} Hz at the strain amplitude of 10^{-1} % (LVR ensured). The performance of the magnetic hydrogels was analyzed in the absence of magnetic field (off-state), and under various magnetic fields (on-state) generated using the power source (PS/MRD/5A), in which the coil current was

step-wise increased producing the magnetic fields up to $438\,\mathrm{kA \cdot m^{-1}}$. To ensure a contact between the PP20 and the POx-based hydrogels, the compressive normal force of 0.1 N was applied and kept constant during the measurements. To minimize the evaporation of the samples, all the measurements were initiated immediately after taking water-equilibrated POx-based gels out of the medium. The constant temperature of $23\pm0.1^\circ$C was provided by the thermostatic device (Julabo FS18, Germany) with a circulating liquid medium.

2.8 Cell lines and growth media. The cytotoxicity and cultivation studies were performed using mice fibroblasts 3T3 (DSMZ, Braunschweig). The 3T3 cells were cultivated in Dulbecco's Modified Eagle Medium (DMEM) supplemented with 10% Fetal Bovine Serum (FBS), L-glutamine (2 mmol), streptomycin (100 µg/mL), penicillin (100 IU/mL), further referred as full DMEM. All chemicals were purchased from Gibco (Life Technologies, USA). The cells were cultivated at 37°C, and 5% CO_2. The cells were trypsinized and the medium was changed every 3 days.

2.9 Cytotoxicity study. Cell toxicity studies were conducted in accordance with the ISO 10993-5 and ISO 10993-12 on mice fibroblast cell line 3T3. All the experiments were performed in pentaplicates, with the non-treated cells as a negative control.
Toxicity of extracts. The dry gels were sterilized by UV light for 30 min, then immersed into full DMEM medium. The final volume of the extraction medium was 1 mL per 0.1 g of dry gel, plus additional volume absorbed by the gel (calculated from the equilibrium SD). The gels were extracted for 24 h at 37°C. Fibroblast cells were seeded on 96-well plate with the seeding density 5 000 cells/well and cultivated for 24 h. The medium was then replaced by the extracts from the POx-based hydrogels and their magnetic analogues. The cells were incubated for additional 24 h and their viability was evaluated by MTT cytotoxicity assay. MTT dissolved in

full DMEM (0.5 mg/mL) was added into the wells for 2 h, and then removed. Formazan crystals were dissolved in 100 µL of DMSO and measured using a plate reader (Labsystems Multiskan MS, Thermo Labsystems, USA) operating at a wavelength of 595 nm. The cell viability was expressed as the percentage of control cells, mean values and standard deviation from quadruplicates.

Direct contact toxicity. For the direct contact toxicity, the cells were seeded into 24-well plate with the seeding density of 20 000 cells/well. The dry gels were sterilized by UV light for 30 min from each side, and then immersed into DMEM medium with 10% FBS serum and incubated for 24 h at 37°C to allow swelling. The cylindrical samples with a diameter of 6 mm were cut from the POx gels and gently placed on the top of the cell layer. The gels covered approx. 14% of the well surface. The cells were incubated with the gels for 24 h, then the medium was removed and MTT dye was added (0.5 g/L) for 2 h. After the incubation period, the morphology of treated cells was evaluated using the optical microscope (OPTIKA, Italy).

3. Results and discussion

3.1 Synthesis. The POx-based hydrogels, and their magnetic analogues were prepared via living cationic ring-opening copolymerization of EtOx and bi-functional OctBisOx acting as a cross-linker. As known, the POx gels can be cross-linked using a plethora of strategies, however short aliphatic chain bis(2-oxazoline) cross-linkers such as OctBisOx were found to possess low cytotoxicity towards fibroblast cells [15,20]. Moreover, the POx-based hydrogels cross-linked using the OctBisOx exhibited superior mechanical properties when compared to their variants cross-linked using 1,4-butylene-2,2'-bis(2-oxazoline) or 1,6-hexamethylene-2,2'-bis(2-oxazoline). Due to these conclusive facts, OctBisOx was selected as a suitable cross-linker for the preparation of magnetic hydrogels. The molar ratio of the monomer to cross-linker was carefully selected based on the results of our previous work [15]. In this work,

EtOx:OctBisOx molar ratio was set to 98:2, since higher amounts of the cross-linker make the washing procedure more problematic, leading to increased cytotoxicity of the hydrogels. As the POx-based hydrogels were prepared using living cationic copolymerization, which is expected to proceed until the full monomer conversion, high yields (more than 90 %) were expected [15]. Herein, slightly lower yield (decreased by ca. 20 %), further expressed as the gel contents, was observed for neat hydrogel (Tab. 1). This decrease might be explained as a consequence of larger synthesis batches in comparison to the preceding ones. Previously, we experienced similar problems with scaling-up the polymerization reaction of triblock copoly(2-oxazoline)s, which led to higher dispersities and issues with the fractionation of the samples during their purification [21].

For the preparation of magnetic hydrogels, the CI particles were suspended in a liquid-state mixture of monomer and the cross-linker prior to the polymerization. Three different amounts of the CI particles were used (0.8, 1.6, and 2.4 g in 1.5 g of EtOx), which resulted in the concentrations of 5.5, 9, and 16 wt.% of the CI particles in the POx-based hydrogel. The calculation given in Tab. 1 is based on the assumption that all the CI particles were successfully incorporated into the POx-based matrix during the polymerization. The decrease of the gel content was observed after the addition of the CI particles; from 77 % for neat matrix to only 6 % for Gel 3. Based on this result, it can be assumed that the addition of the CI particles negatively affected the polymerization of 2-oxazolines, eventually leading to the uncontrolled process. To explore this assumption, we studied the effect of the CI particles on the polymerization kinetics of the EtOx in benzonitrile, but without employing the cross-linker (Fig. S2). Although the polymerization in the presence of the CI particles proceeded slower when compared to its neat matrix analogue, both polymerizations exhibited the first order kinetics, which proved that living character of the process was preserved. Moreover, the conversions after 1 h were almost identical (ca. 99.5 %) in both cases. In a view of these results,

it can be suggested that lower gel contents (Tab. 1) were caused due to washing off the linear/branched polymer fractions from the POx matrix. On the contrary, the CI particles acted as a mechanical barrier preventing the creation of interconnected network, but without any significant effect on the reaction conversion.

During processing of the MR composites the CI particles represent under certain conditions a chemically-active compound, rather than an inert filler. It was found that they can actively-participate in the cross-linking process of the PDMS [22], and also during the thermo-mechanical degradation of the TPE [23]. Since the polymerization of 2-oxazolines possesses the cationic character, the mechanism of the CI particle interaction with the reactive species is expected to be different. Presumably, the growing POx chains can be potentially terminated on the surface of the CI particles that contains the hydroxyl groups [24], or the termination can be caused due to the presence of the impurities, such as moisture. This could explain a slightly slower polymerization of the EtOx in presence of the CI particles (Fig. S2). Additionally, the POx chains and the CI particles may also form complexes similarly as described in a recent work by Venturini et al.[25], where the authors developed one step synthesis of the iron oxide nanoparticles coated by the POx chains. Finally, let us mention that also other fillers were reported to affect the polymerization processes of the POx-based composites. Tasdelen's group [26] reported the increased polymer dispersities in the POx-clay nanocomposites when compared to filler-free matrix, which was explained as a consequence of chain transfer reactions.

Tab. 1: Characteristics of prepared samples. The gel content was calculated as $\frac{\frac{w_{sw}}{SD+1}-w_{CI}}{w_{feed}} \times 100$, where w_{sw} and SD are defined as above, while w_{CI} and w_{feed} denote weight

of the CI particles, and weight of monomers in the feed, respectively. The amount of the CI

particles in swollen gel was calculated as $\frac{w_{CI}}{w_{sw}} \times 100$, where w_{CI} and w_{sw} are defined as above.

Sample ID	Weight of the CI in the feed (g)	CI concentration in the swollen state		Gel content (%)
		(wt.%)	(vol.%)	
Matrix	0.0	0.0	0.0	~77
Gel 1	0.8	5.5	0.8	~50
Gel 2	1.6	9.0	1.3	~16
Gel 3	2.4	16.0	2.4	~6

3.2 Swelling. Swelling can be considered as a fundamental property of the hydrogels. In this

study, swelling of the POx-based gels was investigated in different solvents, and their

equilibrium SD (after 24 h in an excess of selected solvent) was compared. First, we note that

neat matrix exhibited slightly higher SD in water when compared to our previous study [15]

(17±0.5 vs. 12.5±0.9). This result correlates with the already-mentioned decrease of the gel

content, which can be connected to less efficient polymerization reaction. The prepared gels

swell comparably in all tested solvents with different polarity (Fig. 2), thus they can be referred

as the amphigels. The SD obtained in PBS was slightly lower than that in distilled water, even

though the POx-based hydrogels belong to the non-ionic group of materials, and they should

not be sensitive to ionic strength of the solution. Nevertheless, similar results were already

reported and may be explained as a consequence of unreacted POx rings [15,27]. After the

addition of the CI particles, the SD of the gels noticeably decreased, which is in accordance
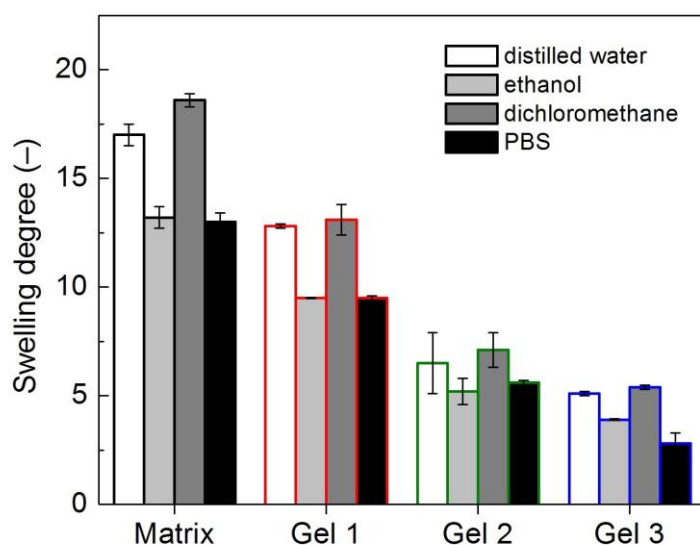
with a recent study on alginate ferrogels [11].

Fig. 2: Equilibrium SD of the POx-based hydrogel, and its magnetic analogues (Gel 1–3) determined by the gravimetric analysis in different liquids.

3.3 Microstructure analysis. The microstructure of the fabricated POx-based magnetic gels was studied using the SEM in a combination with CT. Figure 3 shows the SEM micrograph of neat POx matrix and representative freeze-dried sample (Gel 2). As can be seen, the sample was characterized by the open-porosity with quite complex pore geometry, while the CI particles were well-distributed inside the POx-based matrix. In more details, the particles formed locally-percolated networks consisted of relatively thin (below $10\,\mu$m) particle structures with distinguishable primary particles. Such structures were developed during the hydrogel preparation and their position was fixed upon the cross-linking process. The same characteristics were observed for all magnetic gels (Gel 1–3) regardless the CI concentration (Fig. S3), which indicates a successful fabrication process of these composites.
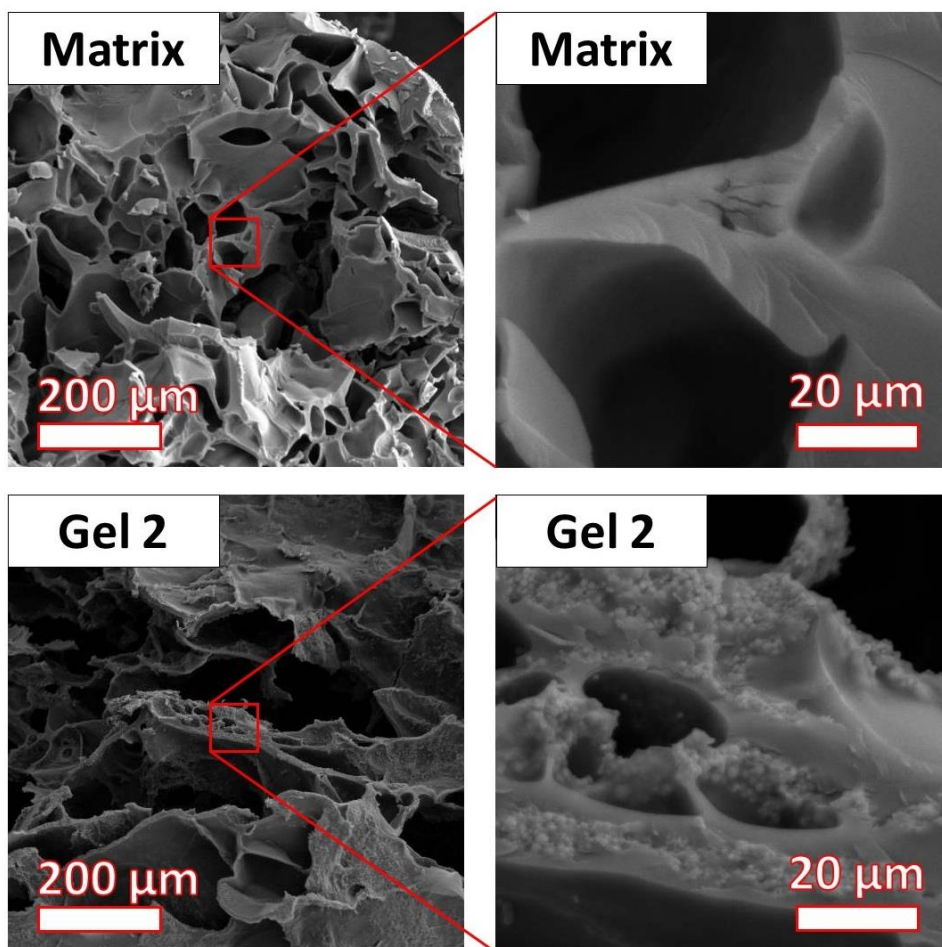
Fig. 3: SEM micrographs and magnified-view regions of neat POx-based matrix, and its magnetic analogue (Gel 2).

The EDX spectra were recorded to verify the presence of the CI particles inside the gels. As seen in Fig. 4, the elemental analysis confirmed the existence of the expected elements represented by C, N, O inside neat POx-based matrix. In the case of magnetic gel, strong signal for Fe indicated the enrichment of the matrix by the CI particles, which provided enough evidence for their successful incorporation. In both cases, the presence of Au signal comes from the sputtered conductive layer.
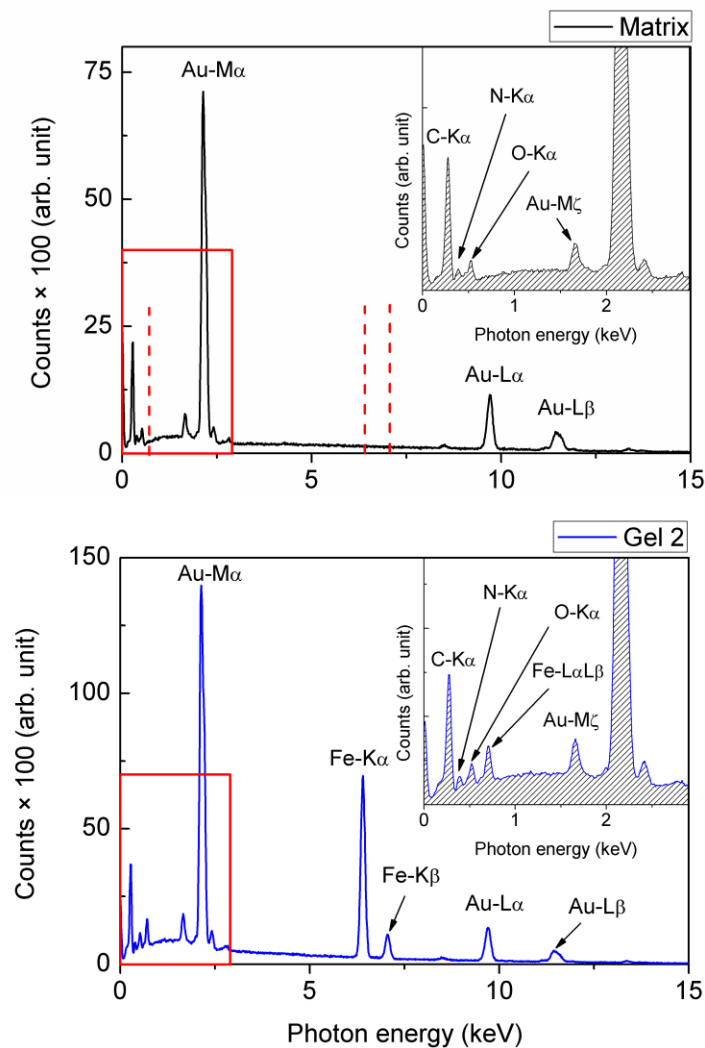
Fig. 4: EDX spectra of neat POx-based matrix, and its magnetic analogue (Gel 2). Spectra were taken from the areas magnified as a part of Fig. 3.

The CT was performed on water-equilibrated POx-based hydrogels and their freeze-dried analogues in order to investigate the pore distribution thorough the volume. Before analyzing the images, it should be mentioned that the individual CI particles were not apparent in the CT scans (resolution of 1 voxel = $10 \times 10 \times 10$ μm) as their diameter was below the resolution limit of the device. Despite that, the pore structure was clearly observable. Figure 5 shows the 2D cross-sectional images together with the corresponding 3D models of Gel 2. As indicated above, the hydrogel was generally characterized by open-porosity. It should be emphasized that

the porous structure was revealed also for the original hydrated gel (without freeze-drying), which proves that pores were formed during the gel synthesis. This is contrary to the other types of the POx gels, e.g., formed by thiol-ene reaction, which exhibited the non-porous structure [28], and the pores had to be introduced via freeze-drying [29]. Further, the data was quantified in detail using digital image processing (Tab. 2). The total porosity roughly decreased after freeze-drying, which proves high water-holding capability of the gels. Moreover, the vast majority of pores had the open structure, while the amount of closed pores was negligible (less than 1% of the volume). To conclude, based on the SEM/EDX and CT observations, it can be asserted that POx-based magnetic gels were successfully fabricated despite possible difficulties accompanying the production of micron-sized high-density particulate gel systems [1]. Such high-porosity materials with the interconnected pores can found the utilization in biomedical applications, as constructs which can be seeded by the cells to promote their migration and proliferation [29].
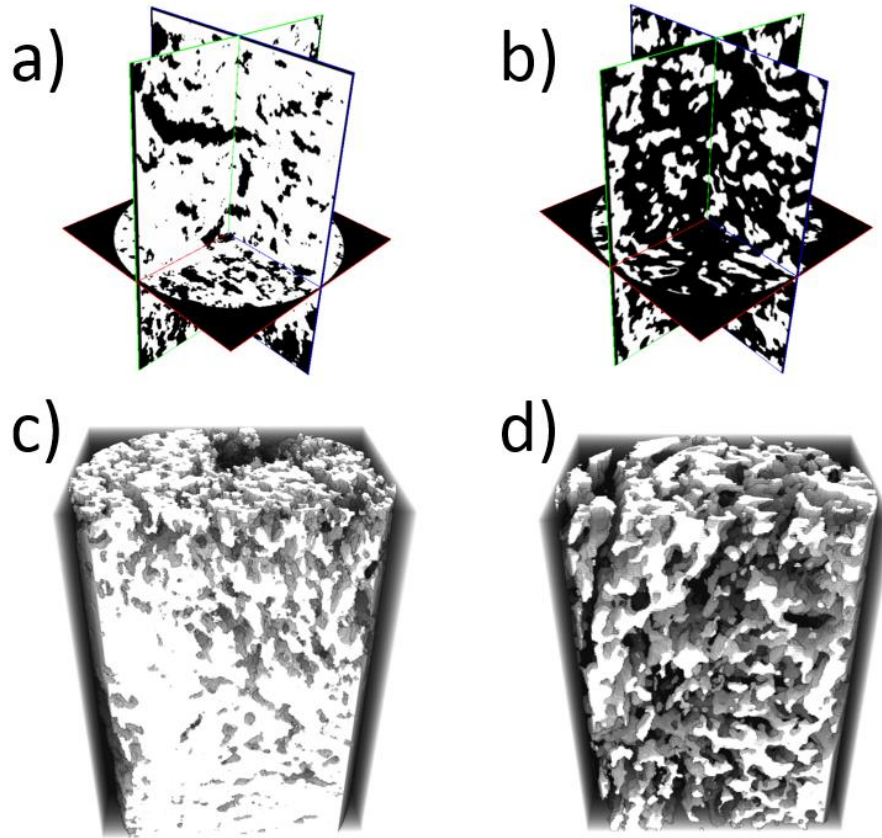
Fig. 5: The reconstructed CT images of Gel 2: in the freeze-dried (*a*, *c*), and in the swollen state (*b*, *d*), respectively. Dimensions of the presented cross sections is 2.27 mm in a diameter, and 3 mm in height.

Tab. 2: Numerical results from 3D image analysis of Gel 2.

Parameter	Unit	Freeze-dried gel	Hydrogel
Analyzed volume	mm^3	11.8	11.8
Pore volume	mm^3	2.6 ± 0.1	7.9 ± 0.1
Porosity	%	22.5 ± 0.3	67.0 ± 1.0
Open pores	%	21.7 ± 0.4	66.8 ± 1.2

3.4 Magnetic properties. The magnetization spectra of water-equilibrated POx-based gels containing the CI particles are presented in Fig. 6. As can be seen, the saturation magnetization was proportional to the CI particle content inside the body of the hydrogels having values close to 10, 17, and 26 emu·g^{-1} for Gel 1–3, respectively. These values seem to be reasonable taking into the account the saturation magnetization of powder-state CI particles (ca. 200 emu·g^{-1}) of the same grade [30] and the content of absorbed water (Tab. 2), which obviously has a significant effect on mass magnetization values [31]. When compared to the hydrogels containing hard magnetic fillers, such as barium ferrites, the presented POx-based analogues exhibited relatively narrow magnetic hysteresis, and higher magnetization values at the same particle content [32]. Indeed, even higher magnetization can be obtained by increasing the particle content, but this may provoke the fragility of the composite [11].
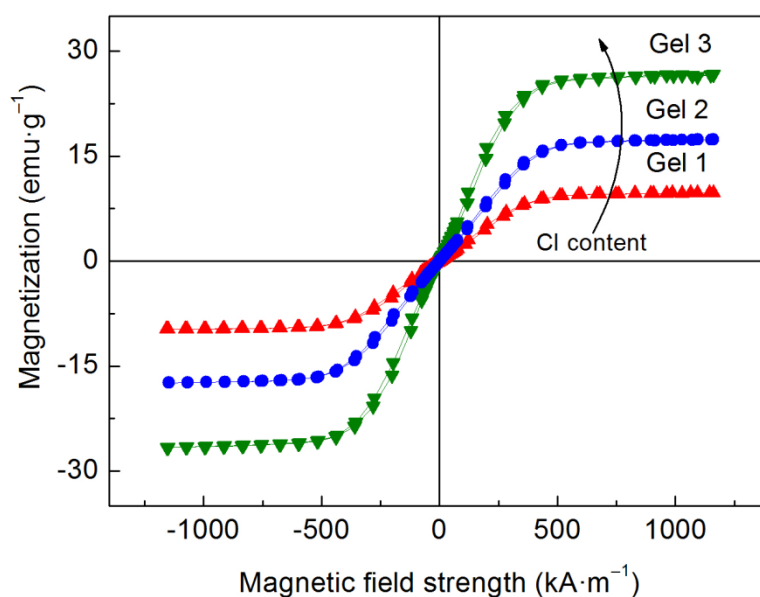

Fig. 6: VSM spectra of the POx-based magnetic hydrogels (Gel 1–3).

A next question arises when dealing with the field-induced motion (displacement and rotation) of the CI particles inside the POx-based matrix. As demonstrated on the magnetorheological suspensions [33], and elastomers [34], the field-induced motion of the embedded particles can

significantly influence the magnetic response of such composites. This phenomenon is associated with re-structuring of the material, when particles aggregate along the field direction due to dipole-dipole interactions, which was, apart from the magnetic measurements, demonstrated by direct microscopy and computer simulations [34]. The manifestation of this phenomenon correlates with the matrix properties, while being negligible in rather stiff systems (shear modulus of hundreds kPa) [35], and more pronounced in the softer ones (shear modulus of tens kPa) [34]. Apart from that, it is also linked to other external conditions, such as temperature, due to temperature-dependence of mechanical properties of the polymers [36]. The evaluation of this phenomenon is preferentially realized via susceptibility representation, which can magnify the artefacts in the low-field region.

As demonstrated in Fig. 3, the CI particles were trapped within the POx-based polymer network, thus considering the elasticity of hydrogels, magnetorestrictive elongation can be expected. Figure 7 displays the susceptibility for all the magnetic gels. A careful examination revealed, that low-field susceptibility values increased by ca. 3-fold across the samples, while being the highest for Gel 3. Despite the fact, that modulus of magnetic gels theoretically depends on the particle volume fraction following the Krieger–Dougherty equation [17], the softest magnetic hydrogel, i.e. Gel 1, exhibited the lowest susceptibility values. Thus, the results clearly show that particle content plays a greater role in grouping the particles then the corresponding increase in matrix stiffness.

Further, the width of the pattern can be also linked to the matrix stiffness (tested for samples with stiffness differing by a magnitude) as observed by Stepanov et al.[34]. In our case, the width of the susceptibility pattern was comparable (Fig. 7), and we assume that the sample re-structuration was completed under magnetic field strength slightly above ± 500 kA·m^{-1}. Finally, let us notice that the local maxima in the susceptibility functions can be associated to the internal particle movement [36], which is the most intense during the low-field magnetization. In this

sense, the intensity of this artefact indicates that Gel 3 experienced the largest field-induced changes on the particle level. Considering such remarkable capability, it can be suggested that the POx-based magnetic hydrogels may found utilization as a platform for the magneto-mechanical stimulation of cells [37].
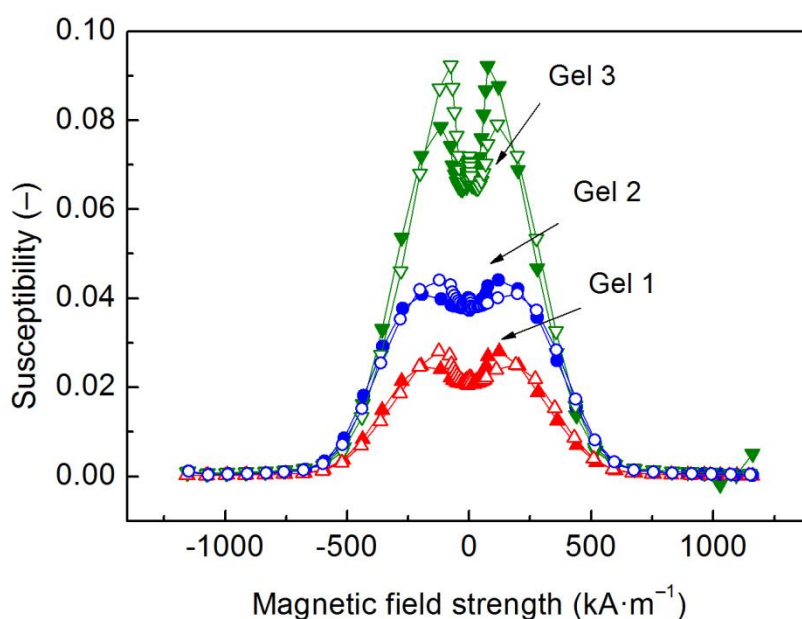

Fig. 7: Differential susceptibility curves of the POx-based magnetic hydrogels (Gel 1–3). The closed/open symbols denote data for decreasing/increasing magnetic field.

3.5 Viscoelasticity and MR activity. Next, we investigated the viscoelastic and the MR response of the POx-based hydrogels. Figure 8a shows the dependences of the storage, G', and the loss, G'', moduli on the applied strain amplitude. As seen, at low strain amplitudes, the G' values exceeded the G'' by more than a decade for all the tested hydrogels, which is a typical feature for the cross-linked polymeric systems [11]. In this region, the both moduli were almost constant defining the LVR. After exceeded a critical strain amplitude, the G' values were strongly decreasing, while the G'' followed the opposite trend, which finally resulted in the crossover of these quantities. Such behavior can be explained due to the existence of the non-linear viscoelasticity region in which, the irreversible deformation of the composite structure

occurs [10]. The friction between the particles and possible rupture of polymer segments are considered as the main factors responsible for the G'' increase [38]. In neat POx matrix, the former mechanism is not applied, therefore a weaker non-linearity was observed when compared to its particle-based analogues. It is also worth mentioning that the G'' exhibited a peak value, known as the yielding point, at which the dissipation of the energy is maximal [39]. As recently observed on alginate hydrogels [11], the relevance of the G'' peak generally decreases with the concentration of magnetic particles and it virtually disappears for the volume fraction over 0.30. In other words, the destruction of the polymer structure corresponding to the G'' peak becomes relatively less pronounced in highly-filled systems. In our case, this type of behavior was not observed, and the G'' peak was clearly distinguishable, most probably due to low particle loadings (only up to 2.4 vol.%) in the POx-based magnetic hydrogels.

The effect of the CI particle concentration on the viscoelastic parameters was further analyzed. We prefer to interpret this effect using the viscoelastic data in the frequency dependence as displayed in Fig. 8b. As clearly obvious, the gradual increase in the CI particle concentration was accompanied by an appreciable increase of the G' as well as G'' moduli. The increase of the former quantity can be explained based on the fact, that the CI micro-particles represent a rigid inorganic filler with much higher stiffness when compared to the POx matrix [40]. Likewise, the G'' increase was associated to enhanced energy dissipation due to more relevant particle/matrix friction in the concentrated gels [22].

Assuming the certain hypotheses [11], the G' value of the magnetic hydrogel can be estimated theoretically for different particle loadings using the Krieger–Dougherty (K–D) equation. In the case of composites, the K–D formula is analogous to that originally proposed for the viscosity estimation of the suspensions upon the introduction of various amounts of the particles [41]. Here, we use the following expression (Eq. 2):

$$G' = G'_0 \left(1 - \frac{\Phi}{\Phi_{\mathrm{m}}}\right)^{-[\eta]\Phi_{\mathrm{m}}} \tag{2}$$

where the G'_0 is the storage modulus of neat matrix, Φ and Φ_{m} represent the volume fraction of the CI particles and its maximum value, respectively, while $[\eta]$ is the parameter associated with the particle shape having the value of 2.5 for rigid spheres. For the CI particles, the Φ_{m} value is usually set to 0.64, which corresponds to random close-packed arrangement even though they are not perfectly-monodisperse [42]. At this point, we note that besides the particle size, shape, and their volume fraction, also other important factors (not included in the K–D model), such as the particle/matrix interfacial adhesion, affect the final mechanical properties of the particulate composites [40]. Despite that, the K–D prediction was numerously applied in the particle-filled hydrogels with various degree of success. While some authors reported a good agreement between the experimental data and the K–D prediction [17], for some materials, the K–D theory considerably underestimated their G' values [11,43]. The literature suggests that this discrepancy arises due to particle/matrix interactions, which can manifest either as a cohesion force [11] or the cross-linking mechanism [43] depending on the physicochemical properties of the components in the particular system. In the case of the POx-based magnetic hydrogels, the G' values significantly exceeded those predicted by the K–D model, which is in accordance to the latter group of the studies. The underlying mechanism behind this phenomenon can be explained as already-mentioned consequence of possible complexation between the iron and the ligand (Section 3.1), which deactivated cations during the POx polymerization [25]. Nevertheless, the exact mechanism of the particle/matrix interaction is still unclear. At the same time, the increased G' values were attributed to the development of the 3D polymer network with the embedded CI particles interacting with the matrix.

The field dependence of the POx-based magnetic composite was further addressed. Figure 8c shows the example of the MR behavior for the representative Gel 2. As seen, the G' of the material noticeably increased in the presence of magnetic field, which is a typical behavior of

the ferrogels [2], and magnetic elastomer systems in general [4,10,11,22], termed as the MR effect. Although the CI particles were expected to be "locked" in their positions upon the polymerization process, their magnetic-induced re-organization was possible due to matrix elasticity (Fig. 7). The on-state G'' values were also enhanced, however they remained lower than the G' for all the applied magnetic fields.

To analyze the effect of the CI particle concentration on the MR performance, the on-state G' was plotted as a function of magnetic field strength for all tested POx-based magnetic gels (Fig. 8d). As expected, the G' values dominated for the hydrogels with a higher CI particle content embedded inside the POx-based matrix. Besides that, the increasing CI content led to the formation of locally-percolated networks (Fig. 3), thus the enhancement of their MR response occurred as a consequence of collective magnetism caused by the magnetic inter-particle interactions [44].

Finally, the efforts were made to predict the MR effect of the POx-based hydrogels. Their response could not be determined using the magnetic dipolar interaction model known from the MR suspensions [45], as for magnetic hydrogels, the on-state G' is usually predicted using a simple power-law dependence [11]. In the non-cross-linked analogous systems, i.e. MR suspensions, the field-stiffening usually follows $\propto H^{2.0}$ at low magnetic fields [46]. As seen in Fig. 8d, the G' of the POx-based hydrogels followed $\propto H^{<1.5}$ due to the structural differences between both systems. In the magnetic hydrogels, the particles are not well-organized into the straight particle-chains, moreover, their re-organization leading to the local saturation is hindered due to the competition between the magnetic forces and the elastic ones originated in the matrix elasticity. From this perspective, it is reasonable to expect a weaker sensitivity to the external magnetic field. This result is in accordance with that reported by Mitsumata et al.[17] who even observed that a critical particle concentration is necessary to produce any macroscopic stress transfer leading to the G' increase. The authors [17] however used the

carrageenan gel as a matrix possessing relatively-high initial stiffness (over 3 kPa). Most probably, due to lower *G'* of the POx-based matrix, the magnetic hydrogels exhibited a certain MR activity thorough the whole concentration range.
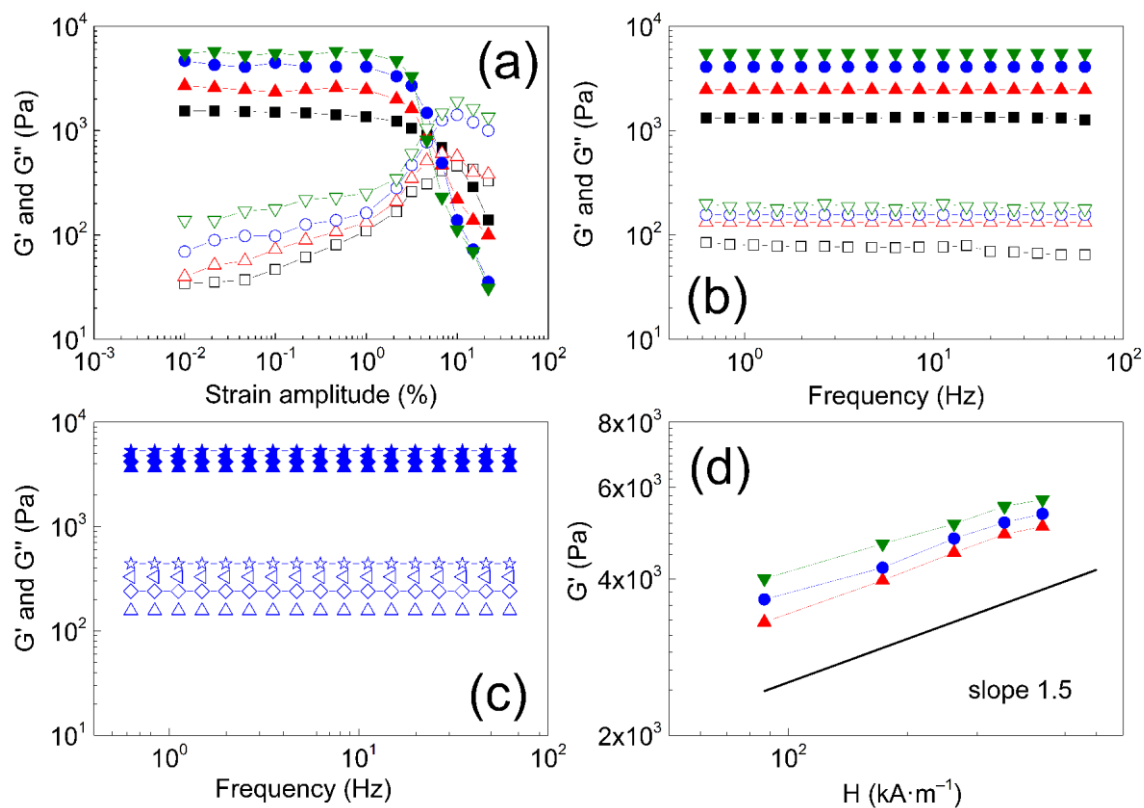

Fig. 8: The storage, *G'* (*solid symbols*), and the loss, *G''* (*open symbols*), moduli of the POx-based matrix (*squares*) and magnetic hydrogels represented by Gel 1 (*up-triangles*), Gel 2 (*circles*), and Gel 3 (*down-triangles*) as a function of strain amplitude (*a*), and frequency (*b*). The MR activity of the representative Gel 2 as a function of frequency (*c*) at the off-state (*up-triangles*), and under 87 (*diamonds*), 171 (*left-triangles*), 438 (*stars*) kA·m^{-1} magnetic field strengths. The *G'* of the magnetic hydrogels (*denoted as above*) as a function of the applied magnetic field strength, where solid line represents slope of 1.5 (*d*).

3.6 Cytotoxicity. Finally, we tested the cytotoxicity of prepared materials towards mice fibroblast 3T3 after 24 h of incubation. The toxicity of the material can be caused by unwashed traces of monomers or solvent used for the polymerization. The toxicity increases with

increasing density of the network (i.e. percentage of cross-linker), as well as the use of less polar cross-linker as we showed in our previous study [15]. In this case, we improved the washing procedure by increasing the number of washing steps and volume of washing liquid, which led to improved biocompatibility of prepared samples. In addition, the gels containing the CI particles exhibited very good biocompatibility towards used cell line, in both the direct contact toxicity and the extract toxicity studies (Fig. 9). The fibroblasts cultivated in a proximity of the hydrogel were well-spread on the surface and they retained normal morphology as displayed in Fig. 10. To conclude, we showed that the fabricated POx-based hydrogels can be considered as non-cytotoxic under the studied conditions, which determines their potential in biomedical and related applications.
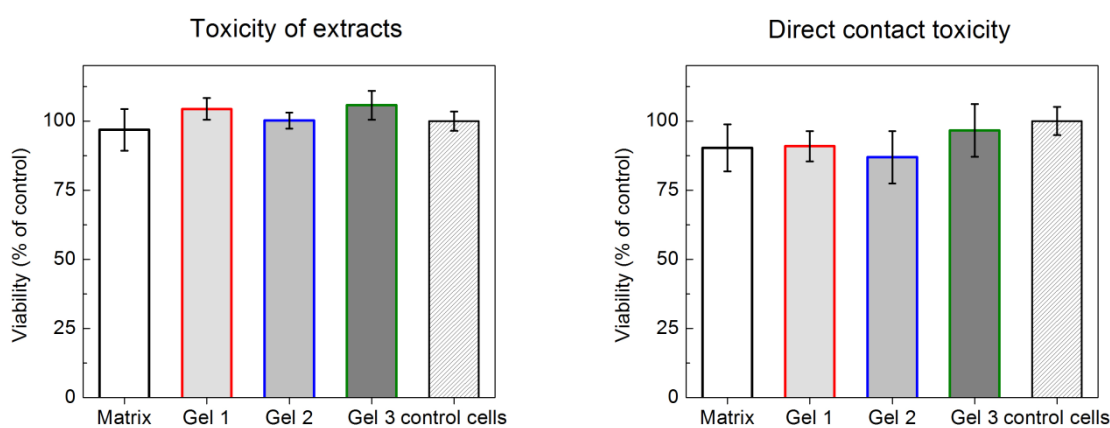

Fig. 9: The cell viability in toxicity of extracts (*left*), and the direct contact toxicity (*right*) testing of the POx-based hydrogel, and its magnetic analogues (Gel 1–3) immersed in full DMEM medium and evaluated via MTT assay after 24 h of incubation with 3T3 fibroblasts.
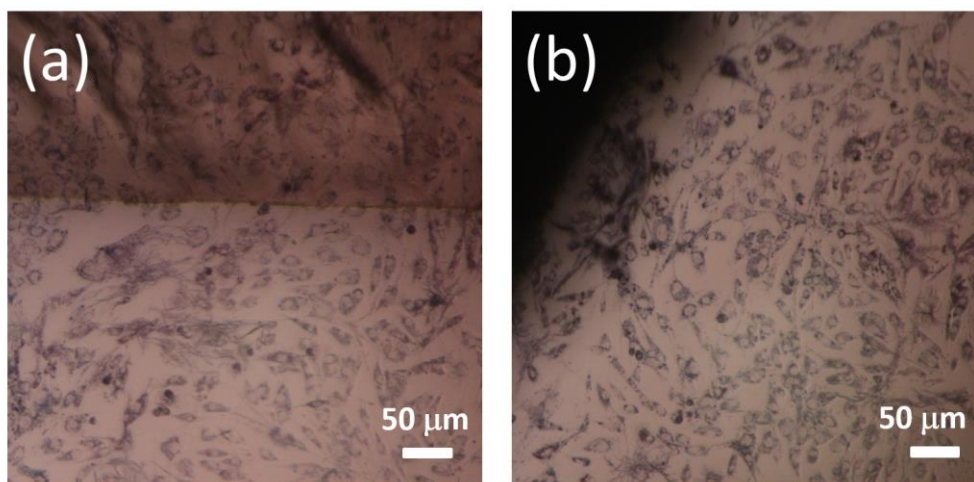
Fig. 10: Representative figures of 3T3 fibroblast cells cultivated for 24 h in the presence of POx-based matrix serving as a reference (*a*), and its magnetic analogue (Gel 2) (*b*).

4. Conclusions

The POx-based magnetic hydrogels were carefully-designed considering a wide library of matrices fabricated previously. Their synthesis was performed via living ring-opening cationic polymerization of 2-ethyl-2-oxazoline with 1,8-octamethylene-2,2′-bis(2-oxazoline) in a 98:2 molar ratio. The magnetic activity was introduced by *in-situ* embedding the CI particles into the pre-polymerized matrix. The efficiency of the synthesis expressed as the gel content was decreasing with the increasing content of the CI particles, most probably due to complexation between the cations and the hydroxyl groups on the CI surface. The CT analysis revealed a significant water-holding capability of the hydrogel, its open pore structure, and negligible percentage of closed pores (less than 1%). The POx-based hydrogels exhibited a reasonable mass magnetization, up to $26\ \mathrm{emu \cdot g^{-1}}$ in the swollen state, and remarkable field-induced internal re-organization determining their potential for the magneto-mechanical stimulation of cells. The *G'* of the hydrogels significantly exceeded the prediction of the K–D model, which supported the theory of the particle/matrix interaction. In magnetic fields, the hydrogels exhibited remarkable MR stiffening proportional to their CI concentration. All hydrogels

exhibited excellent cell viability towards the mice fibroblast 3T3 cell line in direct contact cytotoxicity, and the extract toxicity assay (ISO standards) without any significant change in cell morphology. Due to unique combination of properties manifested as high biocompatibility and sensitivity to magnetic fields, the fabricated POx-based hydrogels may found utilization as a smart composite platform in tissue engineering, pharmaceutical or biomedical fields.

References

1.   Hu, K.; Sun, J.F.; Guo, Z.B.; Wang, P.; Chen, Q.; Ma, M.; Gu, N. A Novel Magnetic Hydrogel with Aligned Magnetic Colloidal Assemblies Showing Controllable Enhancement of Magnetothermal Effect in the Presence of Alternating Magnetic Field. *Adv. Mater.* **2015**, *27*, 2507-2514, doi:10.1002/adma.201405757.

2.   Lopez-Lopez, M.T.; Rodriguez, I.A.; Rodriguez-Arco, L.; Carriel, V.; Bonhome-Espinosa, A.B.; Campos, F.; Zubarev, A.; Duran, J.D.G. Synthesis, characterization and in vivo evaluation of biocompatible ferrogels. *J. Magn. Magn. Mater.* **2017**, *431*, 110-114, doi:10.1016/j.jmmm.2016.08.053.

3. Shah, R.; Saha, N.; Kitano, T.; Saha, P. Preparation of CaCO3- Based Biomineralized Polyvinylpyrrolidone- Carboxymethylcellulose Hydrogels and Their Viscoelastic Behavior. *J. Appl. Polym. Sci.* **2014**, *131*, 9, doi:10.1002/app.40237.

4. Hernandez, R.; Zamora-Mora, V.; Sibaja-Ballestero, M.; Vega-Baudrit, J.; Lopez, D.; Mijangos, C. Influence of iron oxide nanoparticles on the rheological properties of hybrid chitosan ferrogels. *J. Colloid Interface Sci.* **2009**, *339*, 53-59, doi:10.1016/j.jcis.2009.07.066.

5. Blyakhman, F.A.; Safronov, A.P.; Zubarev, A.Y.; Shklyar, T.F.; Makeyev, O.G.; Makarova, E.B.; Melekhin, V.V.; Larranaga, A.; Kurlyandskaya, G.V. Polyacrylamide ferrogels with embedded maghemite nanoparticles for biomedical engineering. *Results Phys.* **2017**, *7*, 3624-3633, doi:10.1016/j.rinp.2017.09.042.

6. Zrinyi, M.; Szabo, D. Muscular contraction mimiced by magnetic gels. *Int. J. Mod. Phys. B* **2001**, *15*, 557-563, doi:10.1142/s0217979201005015.

7. Mitsumata, T.; Nagata, A.; Sakai, K.; Takimoto, J. Giant complex modulus reduction of kappa-carrageenan magnetic gels. *Macromol. Rapid Commun.* **2005**, *26*, 1538-1541, doi:10.1002/marc.200500405.

8. Negami, K.; Mitsumata, T. Magnetorheology of Magnetic Poly(vinyl alcohol) Gels with High Mechanical Toughness. *Chem. Lett.* **2010**, *39*, 550-551, doi:10.1246/cl.2010.550.

9. Yu, M.; Ju, B.X.; Fu, J.; Liu, S.Z.; Choi, S.B. Magnetoresistance Characteristics of Magnetorheological Gel under a Magnetic Field. *Ind. Eng. Chem. Res.* **2014**, *53*, 4704-4710, doi:10.1021/ie4040237.

10. Mordina, B.; Tiwari, R.K.; Setua, D.K.; Sharma, A. Impact of graphene oxide on the magnetorheological behaviour of BaFe12O19 nanoparticles filled polyacrylamide hydrogel. *Polymer* **2016**, *97*, 258-272, doi:10.1016/j.polymer.2016.05.026.

11.   Gila-Vilchez, C.; Bonhome-Espinosa, A.B.; Kuzhir, P.; Zubarev, A.; Duran, J.D.G.; Lopez-Lopez, M.T. Rheology of magnetic alginate hydrogels. *J. Rheol.* **2018**, *62*, 1083-1096, doi:10.1122/1.5028137.

12.   Lorson, T.; Lubtow, M.M.; Wegener, E.; Haider, M.S.; Borova, S.; Nahm, D.; Jordan, R.; Sokolski-Papkov, M.; Kabanov, A.V.; Luxenhofer, R. Poly(2-oxazoline)s based biomaterials: A comprehensive and critical update. *Biomaterials* **2018**, *178*, 204-280, doi:10.1016/j.biomaterials.2018.05.022.

13.   Hoogenboom, R.; Schlaad, H. Bioinspired Poly(2-oxazoline)s. *Polymers* **2011**, *3*, 467-488, doi:10.3390/polym3010467.

14.   Kronek, J.; Kronekova, Z.; Luston, J.; Paulovicova, E.; Paulovicova, L.; Mendrek, B. In vitro bio-immunological and cytotoxicity studies of poly(2-oxazolines). *J. Mater. Sci.-Mater. Med.* **2011**, *22*, 1725-1734, doi:10.1007/s10856-011-4346-z.

15.   Zahoranova, A.; Kronekova, Z.; Zahoran, M.; Chorvat, D.; Janigova, I.; Kronek, J. Poly(2-oxazoline) Hydrogels Crosslinked with Aliphatic bis(2-oxazoline)s: Properties, Cytotoxicity, and Cell Cultivation. *J. Polym. Sci. Pol. Chem.* **2016**, *54*, 1548-1559, doi:10.1002/pola.28009.

16.   Arias, J.L.; Lopez-Viota, M.; Ruiz, M.A.; Lopez-Viota, J.; Delgado, A.V. Development of carbonyl iron/ethylcellulose core/shell nanoparticles for biomedical applications. *Int. J. Pharm.* **2007**, *339*, 237-245, doi:10.1016/j.ijpharm.2007.02.028.

17.   Mitsumata, T.; Honda, A.; Kanazawa, H.; Kawai, M. Magnetically Tunable Elasticity for Magnetic Hydrogels Consisting of Carrageenan and Carbonyl Iron Particles. *J. Phys. Chem. B* **2012**, *116*, 12341-12348, doi:10.1021/jp3049372.

18.   Xu, Y.G.; Gong, X.L.; Xuan, S.H.; Zhang, W.; Fan, Y.C. A high-performance magnetorheological material: preparation, characterization and magnetic-mechanic coupling properties. *Soft Matter* **2011**, *7*, 5246-5254, doi:10.1039/c1sm05301a.

19.   Nery, L.; Lefebvre, H.; Fradet, A. Kinetic and mechanistic studies of carboxylic acid-bisoxazoline chain-coupling reactions. *Macromol. Chem. Phys.* **2003**, *204*, 1755-1764, doi:10.1002/macp.200350036.

20.   Rossegger, E.; Schenk, V.; Wiesbrock, F. Design Strategies for Functionalized Poly(2-oxazoline)s and Derived Materials. *Polymers* **2013**, *5*, 956-1011, doi:10.3390/polym5030956.

21.   Zahoranova, A.; Mrlik, M.; Tomanova, K.; Kronek, J.; Luxenhofer, R. ABA and BAB Triblock Copolymers Based on 2-Methyl-2-oxazoline and 2-n-Propyl-2-oxazoline: Synthesis and Thermoresponsive Behavior in Water. *Macromol. Chem. Phys.* **2017**, *218*, 12, doi:10.1002/macp.201700031.

22.   Cvek, M.; Mrlik, M.; Ilcikova, M.; Mosnacek, J.; Munster, L.; Pavlinek, V. Synthesis of Silicone Elastomers Containing Silyl-Based Polymer Grafted Carbonyl Iron Particles: An Efficient Way To Improve Magnetorheological, Damping, and Sensing Performances. *Macromolecules* **2017**, *50*, 2189-2200, doi:10.1021/acs.macromo1.6b02041.

23.   Cvek, M.; Kracalik, M.; Sedlacik, M.; Mrlik, M.; Sedlarik, V. Reprocessing of injection-molded magnetorheological elastomers based on TPE matrix. *Composites Part B: Engineering* **2019**, *172*, 253-261, doi:10.1016/j.compositesb.2019.05.090.

24.   Belyavskii, S.G.; Mingalyov, P.G.; Giulieri, F.; Combarrieau, R.; Lisichkin, G.V. Chemical modification of the surface of a carbonyl iron powder. *Protect. Met.* **2006**, *42*, 244-252, doi:10.1134/s0033173206030064.

25.   Venturini, P.; Fleutot, S.; Cleymand, F.; Hauet, T.; Dupin, J.C.; Ghanbaja, J.; Martinez, H.; Robin, J.J.; Lapinte, V. Facile One-Step Synthesis of Polyoxazoline-Coated Iron Oxide Nanoparticles. *ChemistrySelect* **2018**, *3*, 11898-11901, doi:10.1002/slct.201802234.

26. Ozkose, U.U.; Altinkok, C.; Yilmaz, O.; Alpturk, O.; Tasdelen, M.A. In-situ preparation of poly(2-ethyl-2-oxazoline)/clay nanocomposites via living cationic ring-opening polymerization. *Eur. Polym. J.* **2017**, *88*, 586-593, doi:10.1016/j.eurpolymj.2016.07.004.

27. Chujo, Y.; Sada, K.; Matsumoto, K.; Saegusa, T. Synthesis of nonionic hydrogel, lipogel, and amphigel by copolymerization of 2-oxazolines and a bisoxazoline. *Macromolecules* **1990**, *23*, 1234-1237, doi:10.1021/ma00207a002.

28. Dargaville, T.R.; Forster, R.; Farrugia, B.L.; Kempe, K.; Voorhaar, L.; Schubert, U.S.; Hoogenboom, R. Poly(2-oxazoline) Hydrogel Monoliths via Thiol-ene Coupling. *Macromol. Rapid Commun.* **2012**, *33*, 1695-1700, doi:10.1002/marc.201200249.

29. van der Heide, D.J.; Verbraeken, B.; Hoogenbloom, R.; Dargaville, T.R.; Hickey, D.K. Porous poly (2-oxazoline) scaffolds for developing 3D primary human tissue culture. *Biomaterials and Tissue Technology* **2017**, *1*, doi:10.15761/BTT.1000104.

30. Cvek, M.; Mrlik, M.; Pavlinek, V. A rheological evaluation of steady shear magnetorheological flow behavior using three-parameter viscoplastic models. *J. Rheol.* **2016**, *60*, 687-694, doi:10.1122/1.4954249.

31. Zhao, X.H.; Kim, J.; Cezar, C.A.; Huebsch, N.; Lee, K.; Bouhadir, K.; Mooney, D.J. Active scaffolds for on-demand drug and cell delivery. *Proc. Natl. Acad. Sci. U. S. A.* **2011**, *108*, 67-72, doi:10.1073/pnas.1007862108.

32. Mitsumata, T.; Wakabayashi, T.; Okazaki, T. Particle Dispersibility and Giant Reduction in Dynamic Modulus of Magnetic Gels Containing Barium Ferrite and Iron Oxide Particles. *J. Phys. Chem. B* **2008**, *112*, 14132-14139, doi:10.1021/jp805955j.

33. de Vicente, J.; Bossis, G.; Lacis, S.; Guyot, M. Permeability measurements in cobalt ferrite and carbonyl iron powders and suspensions. *J. Magn. Magn. Mater.* **2002**, *251*, 100-108, doi:10.1016/s0304-8853(02)00484-5.

34. Stepanov, G.V.; Borin, D.Y.; Raikher, Y.L.; Melenev, P.V.; Perov, N.S. Motion of ferroparticles inside the polymeric matrix in magnetoactive elastomers. *J. Phys.-Condes. Matter* **2008**, *20*, 6, doi:10.1088/0953-8984/20/20/204121.

35. Cvek, M.; Mrlik, M.; Sevcik, J.; Sedlacik, M. Tailoring Performance, Damping, and Surface Properties of Magnetorheological Elastomers via Particle-Grafting Technology. *Polymers* **2018**, *10*, 1411.

36. Bodnaruk, A.V.; Brunhuber, A.; Kalita, V.M.; Kulyk, M.M.; Snarskii, A.A.; Lozenko, A.F.; Ryabchenko, S.M.; Shamonin, M. Temperature-dependent magnetic properties of a magnetoactive elastomer: Immobilization of the soft-magnetic filler. *J. Appl. Phys.* **2018**, *123*, 7, doi:10.1063/1.5023891.

37. Ribeiro, C.; Correia, V.; Martins, P.; Gama, F.M.; Lanceros-Mendez, S. Proving the suitability of magnetoelectric stimuli for tissue engineering applications. *Colloid Surf. B-Biointerfaces* **2016**, *140*, 430-436, doi:10.1016/j.colsurfb.2015.12.055.

38. Sorokin, V.V.; Stepanov, G.V.; Shamonin, M.; Monkman, G.J.; Khokhlov, A.R.; Kramarenko, E.Y. Hysteresis of the viscoelastic properties and the normal force in magnetically and mechanically soft magnetoactive elastomers: Effects of filler composition, strain amplitude and magnetic field. *Polymer* **2015**, *76*, 191-202, doi:10.1016/j.polymer.2015.08.040.

39. Moghimi, E.; Jacob, A.R.; Koumakis, N.; Petekidis, G. Colloidal gels tuned by oscillatory shear. *Soft Matter* **2017**, *13*, 2371-2383, doi:10.1039/c6sm02508k.

40. Fu, S.Y.; Feng, X.Q.; Lauke, B.; Mai, Y.W. Effects of particle size, particle/matrix interface adhesion and particle loading on mechanical properties of particulate-polymer composites. *Compos. Pt. B-Eng.* **2008**, *39*, 933-961, doi:10.1016/j.compositesb.2008.01.002.

41.   Krieger, I.M.; Dougherty, T.J. A mechanism for non-Newtonian flow in suspensions
        of rigid spheres. *Transactions of the Society of Rheology* **1959**, *3*, 137-152,
        doi:10.1122/1.548848.

42.   Ruiz-Lopez, J.A.; Hidalgo-Alvarez, R.; de Vicente, J. Towards a universal master
        curve in magnetorheology. *Smart Mater. Struct.* **2017**, *26*, 6, doi:10.1088/1361-
        665X/aa6648.

43.   Bonhome-Espinosa, A.B.; Campos, F.; Rodriguez, I.A.; Carriel, V.; Marins, J.A.;
        Zubarev, A.; Duran, J.D.G.; Lopez-Lopez, M.T. Effect of particle concentration on the
        microstructural and macromechanical properties of biocompatible magnetic hydrogels.
        Soft Matter **2017**, *13*, 2928-2941, doi:10.1039/c7sm00388a.

44.   Smolkova, I.S.; Kazantseva, N.E.; Parmar, H.; Babayan, V.; Smolka, P.; Saha, P.
        Correlation between coprecipitation reaction course and magneto-structural properties
        of iron oxide nanoparticles. *Mater. Chem. Phys.* **2015**, *155*, 178-190,
        doi:10.1016/j.matchemphys.2015.02.022.

45.   Han, Y.; Hong, W.; Faidley, L.A.E. Field-stiffening effect of magneto-rheological
        elastomers. *Int. J. Solids Struct.* **2013**, *50*, 2281-2288,
        doi:10.1016/j.ijsolstr.2013.03.030.

46.   Ginder, J.M.; Davis, L.C.; Elie, L.D. Rheology of magnetorheological fluids: Models
        and measurements. *Int. J. Mod. Phys. B* **1996**, *10*, 3293-3303,
        doi:10.1142/s0217979296001744.